# Aerosol Composition and Sources during the Chinese Spring Festival: Fireworks, Secondary Aerosol, and Holiday Effects

Qi Jiang[1,3], Yele Sun[1,2*], Zifa Wang[1], Yan Yin[2,3]

[1]State Key Laboratory of Atmospheric Boundary Layer Physics and Atmospheric Chemistry, Institute of Atmospheric Physics, Chinese Academy of Sciences, Beijing 100029, China

[2]Collaborative Innovation Center on Forecast and Evaluation of Meteorological Disasters, Nanjing University of Information Science & Technology, Nanjing, 210044, China

[3]Key Laboratory for Aerosol-Cloud-Precipitation of China Meteorological Administration, Nanjing University of Information Science & Technology, Nanjing 210044, China

Correspondence to: sunyele@mail.iap.ac.cn

## Abstract

Aerosol particles were characterized by an Aerodyne Aerosol Chemical Speciation Monitor (ACSM) along with various collocated instruments in Beijing, China to investigate the roles of fireworks (FW) and secondary aerosol in particulate pollution during the Chinese Spring Festival of 2013. Three fireworks events exerting significant and short-term impacts on fine particles ($PM_{2.5}$) were observed on the days of Lunar New Year, Lunar Fifth Day, and Lantern Festival. The FW showed large impacts on non-refractory potassium, chloride, sulfate, and organics in submicron aerosol ($PM_1$ ), of which the FW organics appeared to be emitted mainly in secondary with its mass spectrum resembling to that of secondary organic aerosol (SOA). Pollution events (PEs) and clean periods (CPs) alternated routinely throughout the study. Secondary particulate matter (SPM = SOA + sulfate + nitrate + ammonium) dominated the total $PM_1$ mass on average accounting for 63-82% during nine PEs in this study. The elevated contributions of secondary species during PEs resulted in a higher mass extinction efficiency of $PM_1$ (6.4 $m^2 g^{-1}$) than that during CPs (4.4 $m^2 g^{-1}$). The Chinese Spring Festival also provides a unique opportunity to study the impacts of reduced anthropogenic emissions on aerosol chemistry in the city. The primary species showed ubiquitous reductions during the holiday period with the largest reduction for cooking OA (69%), nitrogen monoxide (54%), and coal combustion OA (28%). The secondary sulfate, however, remained minor change, and the SOA and the total $PM_{2.5}$ even slightly increased. Our results have significant implications that controlling local primary source emissions during PEs, e.g., cooking and traffic activities, might have limited effects on improving air quality in megacity Beijing due to the dominance of SPM from regional transport in aerosol particle composition.

## 1 Introduction

Air pollution caused by fine particles ($PM_{2.5}$) is of great concern in densely populated megacities because of its adverse effects on human health and regional air quality (Molina and Molina, 2004;Chan and Yao, 2008). The health risk of air pollution is greater than expected leading to around 7 million people's death in 2012 according to the latest report by World Health Organization (http://www.who.int/mediacentre/news/releases/2014/air-pollution/en/). The Beijing metropolitan area is one of the most populous megacities in the world with the population reaching 20.69 million by the end of 2012 (Beijing Municipal Bureau of Statistics). According to Beijing Municipal Environmental Protection Bureau, the annual average concentration of $PM_{2.5}$ was 89.5 μg $m^{-3}$ in 2013, which is about 2.5 times the National Ambient Air Quality Standards of China (35 μg $m^{-3}$ for annual average). This suggests severe fine particle pollution in Beijing. Extensive studies have been made recently to investigate the chemical composition and sources of $PM_{2.5}$. The results showed that secondary inorganic aerosol (SIA = sulfate + nitrate + ammonium), coal combustion, traffic emissions (gasoline and diesel), biomass burning, cooking emissions and dust are the major sources of $PM_{2.5}$ (Zheng et al., 2005;Song et al., 2006;Zhang et al., 2013). However, the source contributions varied significantly among different seasons, therefore improving air quality in Beijing remains a great challenge due to the very complex sources and dynamic evolution processes of aerosol particles.

Fine particles from various sources can be either primary from direct emissions, e.g., fossil fuel combustion and biomass burning, or secondary from atmospheric oxidation of gas-phase species. The fireworks (FW) is one of the most important

primary sources that can exert significant and short-time impacts on air quality. The fireworks burning emits a large amount of gaseous pollutants, e.g., sulfur dioxide ($SO_2$) and nitrogen oxide ($NO_x$) (Vecchi et al., 2008;Huang et al., 2012), and also fine particles comprising organic/elemental carbon, sulfate, potassium, chloride and various metals, e.g., copper (Cu), barium (Ba), strontium (Sr) and magnesium (Mg) (Moreno et al., 2007;Wang et al., 2007;Li et al., 2013). The enhanced short-term air pollution by fireworks can substantially increase health risk levels (Godri et al., 2010;Yang et al., 2014) and reduce visibility for hours (Vecchi et al., 2008). Previous studies on chemical characterization of fireworks in China were mostly based on filter measurements with a time resolution of 12 h or 24 h (Wang et al., 2007;Zhang et al., 2010;Feng et al., 2012;Huang et al., 2012;Cheng et al., 2014;Zhao et al., 2014). Considering that the fireworks events usually last less than 12 hours, the filter analysis may introduce large uncertainties in accurate quantification of chemical composition of FW particles due to either the interferences of non-FW (NFW) background aerosols or the difficulties to account for meteorological variations. Drewnick et al. (2006) first conducted real-time size-resolved chemical composition measurements during the New Year's period in Mainz, Germany using an Aerodyne Time-of-Flight Aerosol Mass Spectrometer (ToF-AMS). To our knowledge, there are no such real-time measurements of chemical composition of aerosol particles during fireworks events in China yet, which limits our understanding on the rapid formation and evolution of fireworks events, and also their impacts on particulate matter (PM) pollution.

Secondary aerosol is of more concern compared to primary aerosol because it is formed over regional scales and exerts impacts on air quality over wider areas (Matsui

et al., 2009;DeCarlo et al., 2010). Therefore, extensive studies have been conducted in recent years to characterize the sources and formation mechanisms of secondary aerosol (Yao et al., 2002;Duan et al., 2006;Sun et al., 2006;Wang et al., 2006;Guo et al., 2010;Yang et al., 2011;Sun et al., 2013b;Zhang et al., 2013;Zhao et al., 2013). SIA was observed to contribute a large fraction of $PM_{2.5}$ and played an enhanced role during haze episodes due to the faster heterogeneous reactions associated with higher humidity (Liu et al., 2013;Sun et al., 2013a;Zhao et al., 2013;Sun et al., 2014;Wang et al., 2014). While SIA was relatively well characterized, secondary organic aerosol (SOA) is not well understood (Huang et al., 2014). The recent deployments of Aerodyne Aerosol Mass Spectrometers (AMS) greatly improved our understanding on sources and evolution processes of organic aerosol (OA) in China, and also the different roles of primary organic aerosol (POA) and SOA in PM pollution (Huang et al., 2010;Sun et al., 2010;He et al., 2011;Sun et al., 2012;Sun et al., 2013b;Zhang et al., 2014). While SOA is more significant in summer (Huang et al., 2010;Sun et al., 2010;Sun et al., 2012), POA generally plays a more important role during wintertime (Sun et al., 2013b). Recently, the role of SOA in fine particle pollution during wintertime – a season with frequent occurrences of pollution episodes in Beijing was extensively investigated and the results highlighted the similar importance of SOA to SIA (Sun et al., 2013b;Sun et al., 2014;Zhang et al., 2014). However, the role of SOA in particulate pollution during periods with largely reduced anthropogenic activities is not well known yet (Huang et al., 2012). This study happened to take place in a month with the most important holiday in China, i.e., the Spring Festival. The source emissions (e.g., traffic and cooking) have significant changes due to a large reduction of population and anthropogenic activities in the city. This provides a unique opportunity to investigate how source changes affect aerosol chemistry including

primary emissions and secondary formation in Beijing. Although Huang et al. (2012) investigated such a holiday effect on aerosol composition and optical properties in Shanghai, the data analyses were limited by daily average composition measurements and also the significantly different meteorological conditions between holiday and non-holiday periods.

In this study, an Aerosol Chemical Speciation Monitor (ACSM) along with various collocated instruments was deployed in Beijing during February 2013. The chemical composition of submicron aerosol ($PM_1$) from fireworks is quantified based on the highly time – resolved measurements of non-refractory submicron aerosol (NR-$PM_1$) species (organics, sulfate, nitrate, ammonium, chloride, and potassium) and black carbon. The impacts of fireworks on PM pollution during Chinese Lunar New Year (LNY), Lunar Fifth Day (LFD), and Lantern Festival (LF) are investigated, and the roles of secondary formation in PM pollution are elucidated. Further, the effects of reduced anthropogenic emissions on primary and secondary aerosols in the city are illustrated, which has significant implications for making air pollution control strategies in Beijing.

## 2 Experimental

### 2.1 Sampling site

The measurements in this study were conducted at the Institute of Atmospheric Physics (IAP), Chinese Academy of Sciences (39°58’28’’N, 116°22’16”E), an urban site located between the north third and fourth ring road in Beijing (Sun et al., 2012). Aerosol measurements were performed from 1 February to 1 March 2013 when three episodes with significant influences of fireworks, i.e., Lunar New Year (LNY), Lunar Fifth Day (LFD), and Lantern Festival (LF), were observed (Fig. 1). The

meteorological conditions during the measurement period are reported in Fig. 1. Winds at the ground surface were generally below 2 m $s^{-1}$ and temperature averaged 0.6 °C. Relative humidity (RH) varied periodically with higher values generally associated with higher PM pollution.

## 2.2 Aerosol sampling

The chemical composition of NR-$PM_1$ including organics, sulfate, nitrate, ammonium, and chloride were measured *in situ* by the ACSM at an approximate 15-min time intervals (Ng et al., 2011b). The ACSM has been widely used for long-term and routine aerosol particle composition measurements due to its robustness (Sun et al., 2012;Budisulistiorini et al., 2014;Petit et al., 2014) despite its lower sensitivity and mass resolution compared to previous versions of research-grade AMS (Jayne et al., 2000;DeCarlo et al., 2006). . In this study, the ambient air was drawn inside the sampling room at a flow rate of 3 L $min^{-1}$, of which ~0.1 L $min^{-1}$ was sub-sampled into the ACSM and 0.85 L $min^{-1}$ into a Cavity Attenuated Phase Shift Spectrometer (CAPS) particle extinction monitor (Massoli et al., 2010). A $PM_{2.5}$ cyclone (Model: URG-2000-30ED) was supplied in front of the sampling line to remove coarse particles with aerodynamic diameters larger than 2.5 μm. The aerosol particles were dried by a silica gel dryer (RH < 40%) before entering the ACSM and the CAPS. The ACSM was operated at a scan rate of 500 ms $amu^{-1}$ for the mass spectrometer from *m/z* 10 – 150. Because ACSM cannot detect refractory components, e.g., BC and mineral dust, a two-wavelength Aethalometer (Model AE22, Magee Scientific Corp.) was therefore used to measure refractory BC in $PM_{2.5}$. The light extinction of dry fine particles ($b_{ext}$, 630 nm) was measured at 1 s time resolution with a precision (3 σ) of 1 M $m^{-1}$ by the CAPS monitor. In addition, the mass concentration

of $PM_{2.5}$ was determined by a heated Tapered Element Oscillating Microbalance, TEOM, and the collocated gaseous species (including CO, $SO_2$, NO, $NO_x$ and $O_3$) were measured by various gas analyzers (Thermo Scientific) at 1 min time resolution. A more detailed descriptions of aerosol and gas measurements were given in Sun et al. (2013b).

### 2.3 ACSM data analysis

The ACSM data were analyzed for the mass concentrations and chemical composition of NR-$PM_1$ using standard ACSM software (v 1.5.3.2) written within Igor Pro (WaveMetrics, Inc., Oregon USA). A composition-dependent collection efficiency (CE) recommended by Middlebrook et al.(2012), CE = max (0.45, 0.0833 + 0.9167 × ANMF), was used to account for the incomplete detection due to the particle bouncing effects (Matthew et al., 2008) and the influences caused by high mass fraction of ammonium nitrate (ANMF). Because aerosol particles were overall neutralized ($NH_4^+{}_{measured}/NH_4^+{}_{predicted}$ = 1.01, $r^2$ = 0.99) and also dried before entering the ACSM, the effects of particle acidity and RH would be minor (Matthew et al., 2008;Middlebrook et al., 2012). The default relative ionization efficiencies (RIEs) except ammonium (RIE = 6.5) that was determined from the IE calibration were used in this study..Quantification of $K^+$ is challenging for ACSM because of a large interference of organic $C_3H_3^+$ at *m/z* 39 and also uncertainties caused by surface ionization (Slowik et al., 2010). In this work, we found that *m/z* 39 was tightly correlated with *m/z* 43 that is completely organics during non-fireworks (NFW) periods ($r^2$ = 0.87, slope = 0.45, Fig. S1). However, higher ratios of *m/z* 39/43 during FW periods were observed due to the elevated $K^+$ signal from burning of fireworks. Assuming that *m/z* 39 was primarily contributed by organics during NFW periods, the

187 excess *m/z* 39 signal, i.e., $K^+$, can then be estimated as *m/z* 39 – *m/z* 43 × 0.45. The
188 $^{41}K^+$ at *m/z* 41 was calculated using an isotopic ratio of 0.0722, i.e., $^{41}K^+ = 0.0722 \times$
189 $K^+$. The $K^+$ signal was converted to mass concentration with a RIE of 2.9 that was
190 reported by Drewnick et al. (2006). It should be noted that the quantification of $K^+$ in
191 this study might have a large uncertainty because of the unknown RIE of $K^+$ ($RIE_K$).
192 The $RIE_K$ can vary a lot depending on the tuning of the spectrometer and the
193 temperature of the vaporizer. For example, Slowik et al. (2010) reported a $RIE_K = 10$
194 based on the calibration of pure $KNO_3$ particles using a ToF-AMS, which is much
195 higher than the $RIE_K = 2.9$ obtained from the comparisons of K/S from fireworks and
196 AMS measurements (Drewnick et al., 2006). In addition, the stability of surface
197 ionization (SI) and electron impact (EI) also affects $RIE_K$. We then checked the
198 variations of the ratio of *m/z* 39/*m/z* 23 (two *m/z*'s with similar surface ionization
199 issues). The average ratio of *m/z* 39/23 during LFD and LF is 8.7 and 11.1,
200 respectively, which is close to 9.0 during the NFW periods. The results suggest that
201 the SI/EI ratio was relatively stable throughout the study. Because we didn't have
202 collocated K measurement, $RIE_K = 2.9$ that was estimated from fireworks was used in
203 this study. The quantified $K^+$ during LFD and LF on average contributed 4.5% and
204 4.7% of $PM_1$, respectively, which is close to ~5% ($PM_{2.5}$) reported by Cheng et al.
205 (2014). Also, the large contribution of $K^+$ to $PM_1$ (20.5%) during LNY, likely due to
206 the intensified firework emissions (mainly firecrackers), is consistent with that (17.3%)
207 observed during LNY 2014 in megacity Tianjin (Tian et al., 2014). Using $RIE_K$=10
208 will decrease the $K^+$ concentration by a factor of more than 3, which appears to
209 underestimate $K^+$ a lot. Therefore, $RIE_K = 2.9$ for the quantification of $K^+$ in our study
210 appear to be reasonable. The $KCl^+$ (*m/z* 74) and $^{41}KCl^+/K^{37}Cl^+$ (*m/z* 76) were
211 estimated by the differences between the measured and PMF modeled *m/z* 74 (Fig.

S2). Not surprisingly, the quantified $KCl^+$ highly correlates with $K^+$ ($r^2$ = 0.82, Fig. S2c). The chloride concentration was also biased at *m/z* 35 during some periods (e.g., LNY, Fig. S3), which is likely due to the interferences of NaCl from fireworks. Therefore, $Cl^+$ (*m/z* 35) was recalculated based on its correlation with *m/z* 36 (mainly $HCl^+$ with negligible $C_3^+$ and $^{36}Ar$), i.e., *m/z* 35 = 0.15 × *m/z* 36. The $^{37}Cl^+$ was calculated using an isotopic ratio of 0.323, i.e., $^{37}Cl^+ = 0.323 \times {}^{35}Cl^+$. The comparison of the reconstructed chloride from the default values is shown in Fig. S3b.

The positive matrix factorization (PMF) with the algorithm of PMF2.exe in robust mode (Paatero and Tapper, 1994) was performed on organic aerosol (OA) mass spectra (*m/z* 12 – 120) to resolve distinct OA components from different sources. The PMF results were evaluated with an Igor Pro-based PMF Evaluation Tool (PET, v 2.04) (Ulbrich et al., 2009) following the procedures detailed in Zhang et al. (2011). After a careful evaluation of the spectral profiles, diurnal variations and correlations with external tracers, a 6-factor solution ($Q/Q_{exp}$ = 4.3) was chosen, yielding a hydrocarbon-like OA (HOA), a cooking OA (COA), a coal combustion OA (CCOA), and three oxygenated OA (OOA) components. Because of the absence of collocated measurements to validate the different OOA components, the three OOA components were recombined into one OOA component. The contributions of four OA factors were relatively stable across different fpeak values (average ± 1σ; min – max, Fig. S4): HOA (14±1.6%; 12 – 16%), COA (14±2.8%; 11 – 17%), CCOA (19±2.7%; 15 – 22%), and OOA (51±1.7; 49 – 55%). However, considering the mass spectra of OA factors at fpeak = -1 presented the best correlation with those identified in winter 2011-2012 ($r^2$ = 0.86 – 0.99, Fig. S5) (Sun et al., 2013b), the four OA factors with fpeak = -1 was chosen in this study. The HOA spectrum resembles to that identified

by PMF analysis of high resolution OA mass spectra in Beijing in January 2013 (Zhang et al., 2014) which are both characterized pronounced *m/z* 91 and 115. Although the CCOA spectrum doesn't present similar pronounced *m/z*'s (e.g., 77, 91, 105, and 115) as that resolved at a rural site in Central Eastern China (Hu et al., 2013), it shows more similarity to that resolved in Beijing (Zhang et al., 2014). Also, CCOA correlates better with chloride with an importance source from coal combustion (Zhang et al., 2012) than HOA ($r^2$ = 0.41 vs. 0.24), and also correlates well with *m/z* 60 ($r^2$ = 0.77, Fig. S6) a tracer *m/z* for biomass burning (Cubison et al., 2011). Note that better correlations between HOA+CCOA and BC ($r^2$ = 0.88), $NO_x$ ($r^2$ = 0.77), and CO ($r^2$ = 0.63) than HOA ($r^2$ = 0.36 – 0.47) were observed in this study, which might suggest that coal combustion emissions are also important sources of CO, BC and $NO_x$ during wintertime (Tian et al., 2008;Zhi et al., 2008).. Although COA didn't have external tracers to validate, it is very distinct as suggested by its unique diurnal patterns (two peaks corresponding to meal time) and high *m/z* 55/57 ratio. Similar to our previous study (Sun et al., 2013b), the OOA shows a tight correlation with $NO_3$ ($r^2$ = 0.90) and also a good correlation with $SO_4^{2-}$+$NO_3^-$ ($r^2$ = 0.87). The mass spectral profiles and time series of four OA factors are shown in Fig. S6.

No biomass burning OA (BBOA) was resolved in this study. One of the reasons is that BBOA was likely not an important component of OA (e.g., < 5%), which is unlikely to be resolved accurately by PMF (Ulbrich et al., 2009). Indeed, we didn't observe strong biomass burning influences throughout the study by checking the scatter plot of $f_{60}$ vs. $f_{44}$ (Fig. S7). We found that $f_{60}$ vs. $f_{44}$ in Fig. S7 is outside of the typical biomass burning region (Cubison et al., 2011) for most of the time during this study. Although the average $f_{60}$ (0.42%) is slightly higher than the typical value of $f_{60}$

(~0.3%) in the absence of biomass burning impact (DeCarlo et al., 2008;Ulbrich et al., 2009), it is also likely due to the short range of *m/z* (12 – 120) used for the calculation of $f_{60}$. A summary of other key diagnostic plots of the PMF solution are given in Fig. S8 and Fig. S9.

## 3 Results and discussion

### 3.1 Identification and quantification of fireworks events

Burning of fireworks has been found to emit a large amount of $K^+$, which can be used to identify the FW events (Drewnick et al., 2006;Wang et al., 2007). As shown in Fig. 1 and Fig. 2, three FW events with significantly elevated $K^+$ were observed on the days of Lunar New Year (LNY, 9-10 February), Lunar Fifth Day (LFD, 14 February), and Lantern Festival (LF, 24 February), respectively. All three FW events started approximately at 18:00 and ended at midnight except LNY with a continuous FW impact until 4:00 on the second day (Fig. 2). Fig. 1 shows that the relative humidity was generally below 30% during LNY and LFD. While the wind speed at the ground surface remained consistently below 2 m $s^{-1}$, it was increased to ~ 4 m $s^{-1}$ at the height of 100 m. Also note that there was a wind direction change in the middle of the two events. The meteorological conditions during LF were stagnant with wind speed generally below 2 m $s^{-1}$ across different heights. The relative humidity was ~50% and the temperature averaged 3.5°C.

To estimate the contributions of fireworks, we first assume that the background concentration of each species has a linear variation during FW period. A linear fit was then performed on the 6 h data before and after FW events. The difference between the measured and the fitted value is assumed as the contribution from FW. The typical examples for estimating FW contributions are shown in Fig. S10. It should be noted

that this approach might significantly overestimate the FW contributions of primary species (e.g., HOA, COA, CCOA, and BC) that were largely enhanced during the typical FW periods (18:00 – 24:00) due to the increased local emissions (see Fig. S11 for diurnal variations of aerosol species). However, it should have a minor impact on secondary species (e.g., $SO_4$, $NO_3$, and OOA) because of their relatively stable variations between 18:00-24:00. As shown in Fig.2, all aerosol species showed substantial increases from 15:00 to 21:00 on the day of LNY which coincidently corresponded to a gradual change of wind direction. Therefore, regional transport might have played dominant roles for the evolution of chemical species during this period. For these reasons, only the FW contributions between 23:30, 9 February and 3:30, 10 February when the meteorological conditions were stable were estimated. The FW contributions during LFD might also be overestimated due to the influences of regional transport as suggested by the wind direction change in the middle. Considering above, the contributions estimated in this work would represent the upper limits of FW.

### 3.2 Mass concentration and chemical composition of FW aerosols

Figure 1 shows the time series of mass concentrations of $PM_1$, $PM_{2.5}$, and submicron aerosol species from 1 February to 1 March 2013. Because ACSM cannot measure the metals (e.g., Sr, Ba, Mg, etc.) that were significantly enhanced during FW periods (Wang et al., 2007;Vecchi et al., 2008) , the $PM_1$ in this study refer to NR-$PM_1$ (= Org + $SO_4$ + $NO_3$ + $NH_4$ + Chl+ K + KCl) + BC. The $PM_{2.5}$ showed three prominent FW peaks with the maximum concentration occurring at ~00:30 during LNY and ~21:30 during LFD and LF, respectively. The peak concentration of $PM_{2.5}$ during LNY (775 μg $m^{-3}$) is more than 10 times higher than the China National

Ambient Air Quality Standard (75 μg $m^{-3}$, 24 h average). The average FW-$PM_{2.5}$ mass concentrations during three FW events all exceeded 100 μg $m^{-3}$. These results suggest that fireworks have large impacts on fine particle pollution, yet generally less than half day (approximately 10 h for LNY, and 6 h for LFD and LF). The $PM_1$ also showed increases during the FW periods, yet not as significant as $PM_{2.5}$. In fact the correlation of $PM_1$ versus $PM_{2.5}$ shows much lower $PM_1/PM_{2.5}$ (0.08 – 0.19) ratios during three FW events than that observed during NFW periods (0.90) (Fig. 3). One of the reasons is likely due to the mineral dust component and metals from fireworks that ACSM did not measure. However, the ACSM un-detected metals (e.g., Mg, Sr, and Ba) that are largely enhanced during FW periods generally contribute a small fraction of PM (<2%) (Wang et al., 2007;Vecchi et al., 2008;Kong et al., 2014). Therefore, our results might suggest that a large fraction of aerosol particles from the burning of fireworks was emitted in the size range of 1 – 2.5 μm. Consistently, Vecchi et al. (2008) found the best correlation between the fireworks tracer, Sr, and the particles between 700-800 nm (mobility diameter, $D_m$) which is approximately equivalent to 1.9 – 2.2 μm in $D_{va}$ (vacuum aerodynamic diameter, $D_{va}$) with a density of 2.7 g $cm^{-3}$ (Zhang et al., 2010).

Figure 4 shows the average chemical composition of $PM_1$ and OA from fireworks and also the background composition during LNY, LFD and LF. The background $PM_1$ during LNY and LFD showed typical characteristics of clean periods with high fraction of organics (> ~50%) (Sun et al., 2012;Sun et al., 2013b), whereas that during LF was dominated by SIA (52%). As a comparison, organics constituted the major fraction of FW-$PM_1$, contributing 44 – 55% on average. During LNY, FW exerted large impacts on potassium and chloride whose contributions were

elevated to 21% and 15% of $PM_1$, respectively, from less than 7% (Chl) in the background aerosols. The large increases of potassium and chloride were also observed during LFD and LF, and previous studies in Beijing (Wang et al., 2007;Cheng et al., 2014). As shown in Fig. 4, FW also emitted a considerable amount of sulfate, accounting for 7% - 14% of $PM_1$. Sulfate correlated strongly with $SO_2$ during all three FW events ($r^2$ = 0.49 -0.92). Given that the relative humidity was low, < 30% during LNY and LFD, and ~ 50% during LF, aqueous-phase oxidation of $SO_2$ depending on liquid water content could not play significant roles for the sulfate formation (Sun et al., 2013a). Therefore, sulfate in FW-$PM_1$ was mainly from the direction emissions of FW. Compared to sulfate, FW appeared to show minor impacts on nitrate, for example, 4% and 2% during LNY and LF, respectively. Although nitrate contributed 12% of FW-$PM_1$ during LFD, most of it was likely from regional transport as supported by synchronous increases of all aerosol species associated with a wind direction change in the middle (Fig. 2).

The OOA contributed dominantly to OA during LNY, which is 79% on average (Fig. 4a). As shown in Fig. 5, the mass spectrum of FW-organics is highly similar to that of low-volatility OOA (LV-OOA, $r^2$ = 0.94; $r^2$ = 0.89 by excluding *m/z* 18 and *m/z* 44) (Ng et al., 2011a) indicating that the FW-organics is likely emitted in secondary. Consistently, Drewnick et al. (2006) also found large enhancements of the OOA-related *m/z*'s (e.g., *m/z* 44) during New Year's fireworks, but the HOA-related *m/z*'s (e.g., *m/z* 57) are not significant contributors to FW organics. OOA accounted for a much smaller fraction of OA during LF (28%) due to the large contributions of POA components (72%). Although the OOA contributions varied during three FW events, their absolute concentrations were relatively close ranging from 5.8 to 7.9 μg

$m^{-3}$. It should be noted that our approach might overestimate the POA components in FW-OA because of the influences of NFW sources, in particular during the FW period of LF when the local HOA, COA, and CCOA happened to have large increases. By excluding the POA components in FW-OA, FW on average contributed 15 – 19 μg $m^{-3}$ $PM_1$ during three FW events.

### 3.3 Secondary aerosol and PM pollution

The $PM_1$ (NR-$PM_1$ + BC) varied largely across the entire study with daily average mass concentration ranging from 9.1 to 169 μg $m^{-3}$. The average $PM_1$ mass concentration was 80 (±68) μg $m^{-3}$, which is approximately 20% higher than that observed during winter 2011-2012 (Sun et al., 2013b). Organics composed the major fraction of $PM_1$ accounting for 43%, followed by nitrate (22%), sulfate (14%), ammonium (13%), BC (5%) and chloride (3%). The OA composition was dominated by OOA (53%) with the rest being POA. Compared to winter 2011-2012 (Sun et al., 2013b), this study showed significantly enhanced OOA (53% vs. 31%) and secondary nitrate (22% vs. 16%), indicating that secondary formation have played important roles in the formation of pollution episodes.

Figure 1d shows that submicron aerosol species alternated routinely between pollution events (PEs) and clean periods (CPs) throughout the entire study. The PEs generally lasted ~1 – 2 days except the one on 23 – 28 February that lasted more than 5 days, whereas the CPs were shorter, generally less than 1 day. In total, 9 PEs and 9 CPs were identified in this study (Fig. 1). A statistics of the mass concentrations and mass fractions of aerosol species during 9 PEs is presented in Fig. 6. The average $PM_1$ mass concentration ranged 68 – 179 μg $m^{-3}$ during PEs with the total secondary particulate matter (SPM = OOA + $SO_4$ + $NO_3$ +$NH_4$) accounting for 63 – 82%. The

average mass concentration of SPM for the 9 PEs was 86 (±32) μg $m^{-3}$, which is nearly 3 times that of primary PM (PPM = HOA + COA +CCOA + BC + Chl) (30 ±9.5 μg $m^{-3}$). SPM consistently dominated $PM_1$ across different PM levels (69 – 75%), but generally with higher contributions (up to 81%) during daytime (Fig. 7b). The diurnal cycle of SPM presented a gradual increase from 50 to 70 μg $m^{-3}$ between 10:00 – 20:00, indicating evident photochemical production of secondary species during daytime. It should be also noted that all secondary species showed ubiquitously higher mass concentrations than those of primary species (Fig. 6a).

The SOA generally contributed more than 50% to OA with an average of 55% during PEs except the episode on 3 February (35%). It's interesting to note that the contribution of POA increased as a function of organic loadings which varied from ~35% to 63% when organics was above 80 μg $m^{-3}$ (Fig. 7c). Such behavior is mainly caused by the enhanced CCOA at high organic mass loadings, which was also observed during winter 2011 – 2012 (Sun et al., 2013b). These results suggest that POA played more important roles than SOA in PM pollution during periods with high organic mass loadings (e.g., > 60 μg $m^{-3}$). In fact, POA showed even higher mass concentration than OOA at nighttime (0:00 – 8:00) due to the intensified local emissions, e.g., coal combustion for heating. Despite this, the role of POA in PM pollution was compensated by the elevated secondary inorganic species as a function of PM loadings (Fig. 7a) leading to the consistently dominant SPM across different pollution levels. Figure 8a shows an evidently lower contribution of organics to $PM_1$ during PEs than CPs. The elevated secondary inorganic species during PEs were closely related to the increase of RH (Fig. 1). For example, during the pollution episode on 3 February, the sulfate concentration increased rapidly and became the

major inorganic species when RH was increased from ~60% to > 90%. The gaseous $SO_2$ showed a corresponding decrease indicating aqueous-phase processing of $SO_2$ to form sulfate, consistent with our previous conclusion that aqueous-phase processing could contribute more than 50% of sulfate production during winter 2011-2012 (Sun et al., 2013a).

The compositional differences between PEs and CPs also led to different mass extinction efficiency (MEE, 630 nm) of $PM_1$ (Fig. 8b). The higher MEE (6.4 $m^2$ $g^{-1}$) during PEs than CPs (4.4 $m^2$ $g^{-1}$) is primarily due to the enhanced secondary species, and also likely the increases of aerosol particle sizes although we don't have size data to support it. Similar increases of mass scattering efficiency from clean periods to relatively polluted conditions were also observed previously in Beijing and Shanghai (Jung et al., 2009;Huang et al., 2013). It should be noted that the MEE of $PM_1$ in this study refers to $PM_{2.5}$ $b_{ext}/PM_1$. Considering that $PM_1$ on average contributes ~60-70% of $PM_{2.5}$ in Beijing (Sun et al., 2012;Sun et al., 2013b), the real MEE of $PM_1$ during PEs and CPs would be ~3.8 - 4.5 and ~2.6 - 3.1 $m^2$ $g^{-1}$, respectively.

### 3.4 Holiday Effects on PM Pollution

Figure 9 shows a comparison of aerosol species, gaseous species, and meteorological parameters between holiday (HD) and non-holiday (NHD) periods. The official holiday for the Spring Festival was 9 – 15 February. However, we noted a large decrease of cooking aerosols from 7 February until 19 February (Fig. S6b), whose emissions were expected to be stable under similar meteorological conditions. The decrease of COA was likely due to the reduction of the number of population in Beijing, which agreed with the fact that most migrants from outside Beijing were leaving for hometown before the official holiday. Therefore, 7 – 19 February was

used as a longer holiday for a comparison. It was estimated that approximately half of population (9 million) left Beijing before the Spring Festival (http://news.xinhuanet.com/yzyd/local/20130208/c_114658765.htm). Such a great reduction in human activities would exert a large impact on aerosol composition and sources in the city during holidays. To better investigate the HD effects on PM pollution, the data shown in Fig. 9 excluded the CPs marked in Fig. 1. The data with the CPs included are presented in Fig. S12.

The differences between HD and NHD for primary species varied largely among different species. COA showed the largest reduction (69%) among aerosol species with the average concentration decreasing from 5.8 μg $m^{-3}$ during NHD to 1.8 μg $m^{-3}$ during HD. The contribution of COA to OA showed a corresponding decrease from 12% to 4%. Given the similar meteorological conditions between HD and NHD, e.g., RH (46% vs. 52%) and wind speed (1.3 m $s^{-1}$ vs. 1.2 m $s^{-1}$), the reduction of COA clearly indicated a large decrease of population and the number of restaurants opened during HD. The CCOA showed approximately 30% reduction during HD, and its contribution to OA decreased from 23% to 18%. Not surprisingly, chloride showed a similar reduction as CCOA because it was primarily from coal combustion emissions during wintertime (Sun et al., 2013b). Figure 9 also shows a significant reduction (54%) for NO indicating much less traffic emissions in the city during HD. The HOA, however, even showed a slight increase during HD, which appeared to contradict with the reduction of two combustion-related tracers, BC and CO (~20%). This can be explained by the fact that coal combustion is a large source of BC and CO during heating season (Tian et al., 2008;Zhi et al., 2008). Consistently, BC and CO showed relatively similar reductions to CCOA. Therefore, the minor variation of HOA might

indicate that the number of heavy-duty vehicles and diesel trucks that dominated HOA emissions (Massoli et al., 2012;Hayes et al., 2013) remained little change during HD period although that of gasoline vehicles was largely decreased. It should be noted that HOA showed a large peak on 9 February – the first day of the official holiday (Fig. S6b) when more traffic emissions were expected due to many people leaving for hometown. After that, HOA showed slightly lower concentration during 11 – 17 February than other periods. In fact, the average HOA showed a slight reduction (~5%) during the long holiday period (7 – 19 February) suggesting a small holiday effect on HOA reduction. Together, the total primary aerosol species (PPM) showed an average reduction of 22% because of holiday effects.

Nitrate showed the largest reduction among secondary species by 22% during HD, primarily due to a reduction of its precursors NO and $NO_2$. The results suggest that reducing traffic emissions would help mitigate the nitrate pollution in the city. Compared to nitrate, sulfate showed minor changes (2%) between HD and NHD, and OOA even showed a slight increase (6%) during HD. One of the reasons is that secondary sulfate and OOA were mainly formed over regional scale and less affected by local production, consistent with their relatively flat diurnal cycles (Fig. S11). Ammonium showed a reduction between nitrate and sulfate because ammonium mainly existed in the form of $(NH_4)_2SO_4$ and $NH_4NO_3$. Overall, secondary species showed generally lower reductions than primary species with the total secondary species (SPM) showing an average reduction of 9% during HD. The joint reductions of PPM and SPM led to an average reduction of 13% for $PM_1$ during HD. However, these reductions did not help alleviate the fine particle pollution during HD. The $PM_{2.5}$ excluding FW impacts even showed 27% increase from 96 μg $m^{-3}$ during NHD

to 122 μg $m^{-3}$ during HD. One possible reason is likely due to the increases of aerosol species in the size range of 1 – 2.5 μm during HD period. The longer holiday (LHD, 7 – 19 February) showed similar influences on both primary and secondary species as the official holiday (9 – 15 February). COA, CCOA, and NO are the three species with the largest reductions during LHD (> 50%). However, HOA, $SO_4$, OOA, and $PM_{2.5}$ showed rather small changes (< ±7%). Therefore, results in this study suggest that controlling the primary source emissions, e.g., cooking and traffic emissions in the city can reduce the primary particles largely, yet has limited effects on secondary species and the total fine particle mass. One of the reasons is because the severe PM pollution in Beijing is predominantly contributed by secondary species (see discussions in section 3.3) that are formed over regional scales. Reducing the primary source emissions in local areas would have limited impacts on mitigation of air pollution in the city. Similarly, Guo et al. (2013) reported a large reduction of primary organic carbon (OC) from traffic emissions and coal combustion during the 2008 Olympic Summer Games when traffic restrictions and temporary closure of factories were implemented. However, secondary OC was not statistically different between controlled and non-controlled periods. Our results highlight the importance of implementing joint efforts over regional scales for air pollution control in north China.

## 4 Conclusions

We have characterized the aerosol particle composition and sources during the Chinese Spring Festival in 2013. The average $PM_1$ mass concentration was 80 (±68) μg $m^{-3}$ for the entire study with organics being the major fraction (43%). Nine pollution events and nine clean periods with substantial compositional differences

were observed. The secondary particulate matter (= SOA+ sulfate + nitrate + ammonium) played a dominant role for the PM pollution during nine PEs. The contributions of SPM to $PM_1$ varied from 63% to 82% with SOA on average accounting for ~55% of OA. As a result, the average mass extinction efficiency of $PM_1$ during PEs (6.4 $m^2 g^{-1}$) was higher than that during CPs (4.4 $m^2 g^{-1}$). Three FW events, i.e., LNY, LFD, and LF, were identified, which showed significant and short-term impacts on fine particles, and non-refractory potassium, chloride, and sulfate in $PM_1$. The FW also exerted a large impact on organics that presented mainly in secondary as indicated by its similar mass spectrum to that of oxygenated OA. The holiday effects on aerosol composition and sources were also investigated by comparing the differences between holiday and non-holiday periods. The changes of anthropogenic source emissions during the holiday showed large impacts on reduction of cooking OA (69%), nitrogen monoxide (54%), and coal combustion OA (28%) in the city, yet presented much smaller influences on secondary species. The average SOA and the total $PM_{2.5}$ even increased slightly during the holiday period. Results here have significant implications that controlling the local primary source emissions, e.g., cooking and traffic activities, might have limited effects on improving air quality during polluted days when SPM from regional transport dominated aerosol composition for most of time. Our results also highlight the importance of implementing joint measures over regional scales for mitigation of air pollution in megacity Beijing.

**Acknowledgements**

This work was supported by the National Key Project of Basic Research (2014CB447900), the Strategic Priority Research Program (B) of the Chinese Academy of Sciences (Grant No. XDB05020501), and the National Natural Science Foundation of China (41175108). We thank Huabin Dong, Hongyan Chen, and Zhe Wang's help in data collection, and also the Technical and Service Center, Institute of Atmospheric Physics, Chinese Academy of Sciences for providing meteorological data.

## References

Budisulistiorini, S. H., Canagaratna, M. R., Croteau, P. L., Baumann, K., Edgerton, E. S., Kollman, M. S., Ng, N. L., Verma, V., Shaw, S. L., Knipping, E. M., Worsnop, D. R., Jayne, J. T., Weber, R. J., and Surratt, J. D.: Intercomparison of an Aerosol Chemical Speciation Monitor (ACSM) with ambient fine aerosol measurements in downtown Atlanta, Georgia, Atmos. Meas. Tech., 7, 1929-1941, 10.5194/amt-7-1929-2014, 2014.

Chan, C. K., and Yao, X.: Air pollution in mega cities in China, Atmos. Environ., 42, 1-42, DOI: 10.1016/j.atmosenv.2007.09.003, 2008.

Cheng, Y., Engling, G., He, K.-b., Duan, F.-k., Du, Z.-y., Ma, Y.-l., Liang, L.-l., Lu, Z.-f., Liu, J.-m., Zheng, M., and Weber, R. J.: The characteristics of Beijing aerosol during two distinct episodes: Impacts of biomass burning and fireworks, Environ. Pollut., 185, 149-157, http://dx.doi.org/10.1016/j.envpol.2013.10.037, 2014.

Cubison, M. J., Ortega, A. M., Hayes, P. L., Farmer, D. K., Day, D., Lechner, M. J., Brune, W. H., Apel, E., Diskin, G. S., Fisher, J. A., Fuelberg, H. E., Hecobian, A., Knapp, D. J., Mikoviny, T., Riemer, D., Sachse, G. W., Sessions, W., Weber, R. J., Weinheimer, A. J., Wisthaler, A., and Jimenez, J. L.: Effects of aging on organic aerosol from open biomass burning smoke in aircraft and laboratory studies, Atmos. Chem. Phys., 11, 12049-12064, 10.5194/acp-11-12049-2011, 2011.

DeCarlo, P. F., Kimmel, J. R., Trimborn, A., Northway, M. J., Jayne, J. T., Aiken, A. C., Gonin, M., Fuhrer, K., Horvath, T., Docherty, K. S., Worsnop, D. R., and Jimenez, J. L.: Field-Deployable, High-Resolution, Time-of-Flight Aerosol Mass Spectrometer, Anal. Chem., 78, 8281-8289, 2006.

DeCarlo, P. F., Dunlea, E. J., Kimmel, J. R., Aiken, A. C., Sueper, D., Crounse, J., Wennberg, P. O., Emmons, L., Shinozuka, Y., Clarke, A., Zhou, J., Tomlinson, J., Collins, D. R., Knapp, D., Weinheimer, A. J., Montzka, D. D., Campos, T., and Jimenez, J. L.: Fast airborne aerosol size and chemistry measurements above Mexico City and Central Mexico during the MILAGRO campaign, Atmos. Chem. Phys., 8, 4027-4048, 2008.

558 DeCarlo, P. F., Ulbrich, I. M., Crounse, J., de Foy, B., Dunlea, E. J., Aiken, A. C., Knapp, D.,
559 Weinheimer, A. J., Campos, T., Wennberg, P. O., and Jimenez, J. L.: Investigation of the
560 sources and processing of organic aerosol over the Central Mexican Plateau from aircraft
561 measurements during MILAGRO, Atmos. Chem. Phys., 10, 5257-5280,
562 10.5194/acp-10-5257-2010, 2010.
563 Drewnick, F., Hings, S. S., Curtius, J., Eerdekens, G., and Williams, J.: Measurement of fine
564 particulate and gas-phase species during the New Year's fireworks 2005 in Mainz,
565 Germany, Atmos. Environ., 40, 4316-4327, 10.1016/j.atmosenv.2006.03.040, 2006.
566 Duan, F. K., He, K. B., Ma, Y. L., Yang, F. M., Yu, X. C., Cadle, S. H., Chan, T., and
567 Mulawa, P. A.: Concentration and chemical characteristics of PM2.5 in Beijing, China:
568 2001–2002, Sci. Total Environ., 355, 264-275, 10.1016/j.scitotenv.2005.03.001, 2006.
569 Feng, J., Sun, P., Hu, X., Zhao, W., Wu, M., and Fu, J.: The chemical composition and
570 sources of PM2.5 during the 2009 Chinese New Year's holiday in Shanghai, Atmospheric
571 Research, 118, 435-444, http://dx.doi.org/10.1016/j.atmosres.2012.08.012, 2012.
572 Godri, K. J., Green, D. C., Fuller, G. W., Dall'Osto, M., Beddows, D. C., Kelly, F. J.,
573 Harrison, R. M., and Mudway, I. S.: Particulate oxidative burden associated with firework
574 activity, 21, 8295-8301 pp., 2010.
575 Guo, S., Hu, M., Wang, Z. B., Slanina, J., and Zhao, Y. L.: Size-resolved aerosol
576 water-soluble ionic compositions in the summer of Beijing: implication of regional
577 secondary formation, Atmos. Chem. Phys., 10, 947-959, 10.5194/acp-10-947-2010, 2010.
578 Guo, S., Hu, M., Guo, Q., Zhang, X., Schauer, J. J., and Zhang, R.: Quantitative evaluation of
579 emission controls on primary and secondary organic aerosol sources during Beijing 2008
580 Olympics, Atmos. Chem. Phys., 13, 8303-8314, 10.5194/acp-13-8303-2013, 2013.
581 Hayes, P. L., Ortega, A. M., Cubison, M. J., Froyd, K. D., Zhao, Y., Cliff, S. S., Hu, W. W.,
582 Toohey, D. W., Flynn, J. H., Lefer, B. L., Grossberg, N., Alvarez, S., Rappenglück, B.,
583 Taylor, J. W., Allan, J. D., Holloway, J. S., Gilman, J. B., Kuster, W. C., de Gouw, J. A.,
584 Massoli, P., Zhang, X., Liu, J., Weber, R. J., Corrigan, A. L., Russell, L. M., Isaacman, G.,
585 Worton, D. R., Kreisberg, N. M., Goldstein, A. H., Thalman, R., Waxman, E. M.,
586 Volkamer, R., Lin, Y. H., Surratt, J. D., Kleindienst, T. E., Offenberg, J. H., Dusanter, S.,
587 Griffith, S., Stevens, P. S., Brioude, J., Angevine, W. M., and Jimenez, J. L.: Organic
588 aerosol composition and sources in Pasadena, California during the 2010 CalNex
589 campaign, Journal of Geophysical Research: Atmospheres, 118, 9233–9257,
590 10.1002/jgrd.50530, 2013.
591 He, L.-Y., Huang, X.-F., Xue, L., Hu, M., Lin, Y., Zheng, J., Zhang, R., and Zhang, Y.-H.:
592 Submicron aerosol analysis and organic source apportionment in an urban atmosphere in
593 Pearl River Delta of China using high-resolution aerosol mass spectrometry, J. Geophys.
594 Res., 116, D12304, 10.1029/2010jd014566, 2011.
595 Hu, W. W., Hu, M., Yuan, B., Jimenez, J. L., Tang, Q., Peng, J. F., Hu, W., Shao, M., Wang,
596 M., Zeng, L. M., Wu, Y. S., Gong, Z. H., Huang, X. F., and He, L. Y.: Insights on organic
597 aerosol aging and the influence of coal combustion at a regional receptor site of central
598 eastern China, Atmos. Chem. Phys., 13, 10095-10112, 10.5194/acp-13-10095-2013,
599 2013.

Huang, K., Zhuang, G., Lin, Y., Wang, Q., Fu, J. S., Zhang, R., Li, J., Deng, C., and Fu, Q.: Impact of anthropogenic emission on air quality over a megacity – revealed from an intensive atmospheric campaign during the Chinese Spring Festival, Atmos. Chem. Phys., 12, 11631-11645, 10.5194/acp-12-11631-2012, 2012.

Huang, R.-J., Zhang, Y., Bozzetti, C., Ho, K.-F., Cao, J.-J., Han, Y., Daellenbach, K. R., Slowik, J. G., Platt, S. M., Canonaco, F., Zotter, P., Wolf, R., Pieber, S. M., Bruns, E. A., Crippa, M., Ciarelli, G., Piazzalunga, A., Schwikowski, M., Abbaszade, G., Schnelle-Kreis, J., Zimmermann, R., An, Z., Szidat, S., Baltensperger, U., Haddad, I. E., and Prevot, A. S. H.: High secondary aerosol contribution to particulate pollution during haze events in China, Nature, advance online publication, 10.1038/nature13774, 2014.

Huang, X. F., He, L. Y., Hu, M., Canagaratna, M. R., Sun, Y., Zhang, Q., Zhu, T., Xue, L., Zeng, L. W., Liu, X. G., Zhang, Y. H., Jayne, J. T., Ng, N. L., and Worsnop, D. R.: Highly time-resolved chemical characterization of atmospheric submicron particles during 2008 Beijing Olympic Games using an Aerodyne High-Resolution Aerosol Mass Spectrometer, Atmos. Chem. Phys., 10, 8933-8945, 10.5194/acp-10-8933-2010, 2010.

Huang, Y., Li, L., Li, J., Wang, X., Chen, H., Chen, J., Yang, X., Gross, D. S., Wang, H., Qiao, L., and Chen, C.: A case study of the highly time-resolved evolution of aerosol chemical and optical properties in urban Shanghai, China, Atmos. Chem. Phys., 13, 3931-3944, 10.5194/acp-13-3931-2013, 2013.

Jayne, J. T., Leard, D. C., Zhang, X., Davidovits, P., Smith, K. A., Kolb, C. E., and Worsnop, D. R.: Development of an aerosol mass spectrometer for size and composition analysis of submicron particles, Aerosol Sci. Tech., 33, 49-70, 2000.

Jung, J., Lee, H., Kim, Y. J., Liu, X., Zhang, Y., Hu, M., and Sugimoto, N.: Optical properties of atmospheric aerosols obtained by in situ and remote measurements during 2006 Campaign of Air Quality Research in Beijing (CAREBeijing-2006), J. Geophys. Res., 114, D00G02, 10.1029/2008jd010337, 2009.

Kong, S., Li, L., Li, X., Yin, Y., Chen, K., Liu, D., Yuan, L., Zhang, Y., Shan, Y., and Ji, Y.: The impacts of fireworks burning at Chinese Spring Festival on air quality and human health: insights of tracers, source evolution and aging processes, Atmos. Chem. Phys. Discuss., 14, 28609-28655, 10.5194/acpd-14-28609-2014, 2014.

Li, W., Shi, Z., Yan, C., Yang, L., Dong, C., and Wang, W.: Individual metal-bearing particles in a regional haze caused by firecracker and firework emissions, Sci. Total Environ., 443, 464-469, http://dx.doi.org/10.1016/j.scitotenv.2012.10.109, 2013.

Liu, X. G., Li, J., Qu, Y., Han, T., Hou, L., Gu, J., Chen, C., Yang, Y., Liu, X., Yang, T., Zhang, Y., Tian, H., and Hu, M.: Formation and evolution mechanism of regional haze: a case study in the megacity Beijing, China, Atmos. Chem. Phys., 13, 4501-4514, 10.5194/acp-13-4501-2013, 2013.

Massoli, P., Kebabian, P. L., Onasch, T. B., Hills, F. B., and Freedman, A.: Aerosol Light Extinction Measurements by Cavity Attenuated Phase Shift (CAPS) Spectroscopy: Laboratory Validation and Field Deployment of a Compact Aerosol Particle Extinction Monitor, Aerosol Sci. Tech., 44, 428-435, 10.1080/02786821003716599, 2010.

Massoli, P., Fortner, E. C., Canagaratna, M. R., Williams, L. R., Zhang, Q., Sun, Y., Schwab, J. J., Trimborn, A., Onasch, T. B., Demerjian, K. L., Kolb, C. E., Worsnop, D. R., and

643 Jayne, J. T.: Pollution Gradients and Chemical Characterization of Particulate Matter
644 from Vehicular Traffic Near Major Roadways: Results from the 2009 Queens College Air
645 Quality Study in NYC, Aerosol Sci. Tech., 46, 1201-1218,
646 10.1080/02786826.2012.701784, 2012.
647 Matsui, H., Koike, M., Kondo, Y., Takegawa, N., Kita, K., Miyazaki, Y., Hu, M., Chang, S.
648 Y., Blake, D. R., Fast, J. D., Zaveri, R. A., Streets, D. G., Zhang, Q., and Zhu, T.: Spatial
649 and temporal variations of aerosols around Beijing in summer 2006: Model evaluation
650 and source apportionment, J. Geophys. Res., 114, D00G13, 10.1029/2008jd010906, 2009.
651 Matthew, B. M., Middlebrook, A. M., and Onasch, T. B.: Collection Efficiencies in an
652 Aerodyne Aerosol Mass Spectrometer as a Function of Particle Phase for Laboratory
653 Generated Aerosols, Aerosol Sci. Tech., 42, 884 - 898, 2008.
654 Middlebrook, A. M., Bahreini, R., Jimenez, J. L., and Canagaratna, M. R.: Evaluation of
655 Composition-Dependent Collection Efficiencies for the Aerodyne Aerosol Mass
656 Spectrometer using Field Data, Aerosol Sci. Tech., 46, 258-271, 2012.
657 Molina, M. J., and Molina, L. T.: Megacities and atmospheric pollution, J. Air Waste Manage.
658 Assoc., 54, 644–680, 2004.
659 Moreno, T., Querol, X., Alastuey, A., Cruz Minguillón, M., Pey, J., Rodriguez, S., Vicente
660 Miró, J., Felis, C., and Gibbons, W.: Recreational atmospheric pollution episodes:
661 Inhalable metalliferous particles from firework displays, Atmos. Environ., 41, 913-922,
662 http://dx.doi.org/10.1016/j.atmosenv.2006.09.019, 2007.
663 Ng, N. L., Canagaratna, M. R., Jimenez, J. L., Zhang, Q., Ulbrich, I. M., and Worsnop, D. R.:
664 Real-Time Methods for Estimating Organic Component Mass Concentrations from
665 Aerosol Mass Spectrometer Data, Environ. Sci. Technol., 45, 910-916,
666 10.1021/es102951k, 2011a.
667 Ng, N. L., Herndon, S. C., Trimborn, A., Canagaratna, M. R., Croteau, P. L., Onasch, T. B.,
668 Sueper, D., Worsnop, D. R., Zhang, Q., Sun, Y. L., and Jayne, J. T.: An Aerosol
669 Chemical Speciation Monitor (ACSM) for Routine Monitoring of the Composition and
670 Mass Concentrations of Ambient Aerosol, Aerosol Sci. Tech., 45, 770 - 784, 2011b.
671 Paatero, P., and Tapper, U.: Positive matrix factorization: A non-negative factor model with
672 optimal utilization of error estimates of data values, Environmetrics, 5, 111-126, 1994.
673 Petit, J. E., Favez, O., Sciare, J., Canonaco, F., Croteau, P., Močnik, G., Jayne, J., Worsnop,
674 D., and Leoz-Garziandia, E.: Submicron aerosol source apportionment of wintertime
675 pollution in Paris, France by double positive matrix factorization (PMF2) using an aerosol
676 chemical speciation monitor (ACSM) and a multi-wavelength Aethalometer, Atmos.
677 Chem. Phys., 14, 13773-13787, 10.5194/acp-14-13773-2014, 2014.
678 Slowik, J. G., Stroud, C., Bottenheim, J. W., Brickell, P. C., Chang, R. Y. W., Liggio, J.,
679 Makar, P. A., Martin, R. V., Moran, M. D., Shantz, N. C., Sjostedt, S. J., van Donkelaar,
680 A., Vlasenko, A., Wiebe, H. A., Xia, A. G., Zhang, J., Leaitch, W. R., and Abbatt, J. P. D.:
681 Characterization of a large biogenic secondary organic aerosol event from eastern
682 Canadian forests, Atmos. Chem. Phys., 10, 2825-2845, 2010.
683 Song, Y., Zhang, Y., Xie, S., Zeng, L., Zheng, M., Salmon, L. G., Shao, M., and Slanina, S.:
684 Source apportionment of PM2.5 in Beijing by positive matrix factorization, Atmos.
685 Environ., 40, 1526-1537, DOI: 10.1016/j.atmosenv.2005.10.039, 2006.

686 Sun, J., Zhang, Q., Canagaratna, M. R., Zhang, Y., Ng, N. L., Sun, Y., Jayne, J. T., Zhang, X.,
687 Zhang, X., and Worsnop, D. R.: Highly time- and size-resolved characterization of
688 submicron aerosol particles in Beijing using an Aerodyne Aerosol Mass Spectrometer,
689 Atmos. Environ., 44, 131-140, 2010.
690 Sun, Y., Zhuang, G., Tang, A., Wang, Y., and An, Z.: Chemical Characteristics of $PM_{2.5}$ and
691 $PM_{10}$ in Haze-Fog Episodes in Beijing, Environ. Sci. Technol., 40, 3148-3155, 2006.
692 Sun, Y., Jiang, Q., Wang, Z., Fu, P., Li, J., Yang, T., and Yin, Y.: Investigation of the Sources
693 and Evolution Processes of Severe Haze Pollution in Beijing in January 2013, Journal of
694 Geophysical Research: Atmospheres, 119, 4380-4398, 10.1002/2014JD021641, 2014.
695 Sun, Y. L., Wang, Z., Dong, H., Yang, T., Li, J., Pan, X., Chen, P., and Jayne, J. T.:
696 Characterization of summer organic and inorganic aerosols in Beijing, China with an
697 Aerosol Chemical Speciation Monitor, Atmos. Environ., 51, 250-259,
698 10.1016/j.atmosenv.2012.01.013, 2012.
699 Sun, Y. L., Wang, Z., Fu, P., Jiang, Q., Yang, T., Li, J., and Ge, X.: The Impact of Relative
700 Humidity on Aerosol Composition and Evolution Processes during Wintertime in Beijing,
701 China, Atmos. Environ., 77, 927–934, http://dx.doi.org/10.1016/j.atmosenv.2013.06.019,
702 2013a.
703 Sun, Y. L., Wang, Z. F., Fu, P. Q., Yang, T., Jiang, Q., Dong, H. B., Li, J., and Jia, J. J.:
704 Aerosol composition, sources and processes during wintertime in Beijing, China, Atmos.
705 Chem. Phys., 13, 4577-4592, 10.5194/acp-13-4577-2013, 2013b.
706 Tian, L., Lucas, D., Fischer, S. L., Lee, S. C., Hammond, S. K., and Koshland, C. P.: Particle
707 and Gas Emissions from a Simulated Coal-Burning Household Fire Pit, Environ. Sci.
708 Technol., 42, 2503-2508, 10.1021/es0716610, 2008.
709 Tian, Y. Z., Wang, J., Peng, X., Shi, G. L., and Feng, Y. C.: Estimation of the direct and
710 indirect impacts of fireworks on the physicochemical characteristics of atmospheric
711 PM10 and PM2.5, Atmos. Chem. Phys., 14, 9469-9479, 10.5194/acp-14-9469-2014,
712 2014.
713 Ulbrich, I. M., Canagaratna, M. R., Zhang, Q., Worsnop, D. R., and Jimenez, J. L.:
714 Interpretation of organic components from Positive Matrix Factorization of aerosol mass
715 spectrometric data, Atmos. Chem. Phys., 9, 2891-2918, 2009.
716 Vecchi, R., Bernardoni, V., Cricchio, D., D'Alessandro, A., Fermo, P., Lucarelli, F., Nava, S.,
717 Piazzalunga, A., and Valli, G.: The impact of fireworks on airborne particles, Atmos.
718 Environ., 42, 1121-1132, 10.1016/j.atmosenv.2007.10.047, 2008.
719 Wang, Y., Zhuang, G., Sun, Y., and An, Z.: The variation of characteristics and formation
720 mechanisms of aerosols in dust, haze, and clear days in Beijing, Atmos. Environ., 40,
721 6579-6591, 2006.
722 Wang, Y., Zhuang, G., Xu, C., and An, Z.: The air pollution caused by the burning of
723 fireworks during the lantern festival in Beijing, Atmos. Environ., 41, 417-431,
724 10.1016/j.atmosenv.2006.07.043, 2007.
725 Wang, Y., Yao, L., Wang, L., Liu, Z., Ji, D., Tang, G., Zhang, J., Sun, Y., Hu, B., and Xin, J.:
726 Mechanism for the formation of the January 2013 heavy haze pollution episode over
727 central and eastern China, Sci. China Earth Sci., 57, 14-25, 10.1007/s11430-013-4773-4,
728 2014.

729 Yang, F., Tan, J., Zhao, Q., Du, Z., He, K., Ma, Y., Duan, F., and Chen, G.: Characteristics of
730 PM2.5 speciation in representative megacities and across China, Atmos. Chem. Phys., 11,
731 5207-5219, 10.5194/acp-11-5207-2011, 2011.
732 Yang, L., Gao, X., Wang, X., Nie, W., Wang, J., Gao, R., Xu, P., Shou, Y., Zhang, Q., and
733 Wang, W.: Impacts of firecracker burning on aerosol chemical characteristics and human
734 health risk levels during the Chinese New Year Celebration in Jinan, China, Sci. Total
735 Environ., 476–477, 57-64, http://dx.doi.org/10.1016/j.scitotenv.2013.12.110, 2014.
736 Yao, X., Chan, C. K., Fang, M., Cadle, S., Chan, T., Mulawa, P., He, K., and Ye, B.: The
737 water-soluble ionic composition of PM2.5 in Shanghai and Beijing, China, Atmos.
738 Environ., 36, 4223-4234, Doi: 10.1016/s1352-2310(02)00342-4, 2002.
739 Zhang, H., Wang, S., Hao, J., Wan, L., Jiang, J., Zhang, M., Mestl, H. E. S., Alnes, L. W. H.,
740 Aunan, K., and Mellouki, A. W.: Chemical and size characterization of particles emitted
741 from the burning of coal and wood in rural households in Guizhou, China, Atmos.
742 Environ., 51, 94-99, 10.1016/j.atmosenv.2012.01.042, 2012.
743 Zhang, J. K., Sun, Y., Liu, Z. R., Ji, D. S., Hu, B., Liu, Q., and Wang, Y. S.: Characterization
744 of submicron aerosols during a month of serious pollution in Beijing, 2013, Atmos. Chem.
745 Phys., 14, 2887-2903, 10.5194/acp-14-2887-2014, 2014.
746 Zhang, M., Wang, X., Chen, J., Cheng, T., Wang, T., Yang, X., Gong, Y., Geng, F., and Chen,
747 C.: Physical characterization of aerosol particles during the Chinese New Year's firework
748 events, Atmos. Environ., 44, 5191-5198, 10.1016/j.atmosenv.2010.08.048, 2010.
749 Zhang, Q., Jimenez, J., Canagaratna, M., Ulbrich, I., Ng, N., Worsnop, D., and Sun, Y.:
750 Understanding atmospheric organic aerosols via factor analysis of aerosol mass
751 spectrometry: a review, Anal. Bioanal. Chem., 401, 3045-3067,
752 10.1007/s00216-011-5355-y, 2011.
753 Zhang, R., Jing, J., Tao, J., Hsu, S. C., Wang, G., Cao, J., Lee, C. S. L., Zhu, L., Chen, Z.,
754 Zhao, Y., and Shen, Z.: Chemical characterization and source apportionment of PM2.5 in
755 Beijing: seasonal perspective, Atmos. Chem. Phys., 13, 7053-7074,
756 10.5194/acp-13-7053-2013, 2013.
757 Zhao, S., Yu, Y., Yin, D., Liu, N., and He, J.: Ambient particulate pollution during Chinese
758 Spring Festival in urban Lanzhou, Northwestern China, Atmospheric Pollution Research,
759 5, 335-343, doi: 10.5094/APR.2014.039, 2014.
760 Zhao, X. J., Zhao, P. S., Xu, J., Meng, W., Pu, W. W., Dong, F., He, D., and Shi, Q. F.:
761 Analysis of a winter regional haze event and its formation mechanism in the North China
762 Plain, Atmos. Chem. Phys., 13, 5685-5696, 10.5194/acp-13-5685-2013, 2013.
763 Zheng, M., Salmon, L. G., Schauer, J. J., Zeng, L., Kiang, C. S., Zhang, Y., and Cass, G. R.:
764 Seasonal trends in PM2.5 source contributions in Beijing, China, Atmos. Environ., 39,
765 3967-3976, DOI: 10.1016/j.atmosenv.2005.03.036, 2005.
766 Zhi, G., Chen, Y., Feng, Y., Xiong, S., Li, J., Zhang, G., Sheng, G., and Fu, J.: Emission
767 characteristics of carbonaceous particles from various residential coal-stoves in China,
768 Environ. Sci. Technol., 42, 3310-3315, 2008.

769

**Figure Captions:**

**Fig. 1.** Time series of meteorological parameters (a) relative humidity (RH) and temperature (T); (b) wind direction (WD) and wind speed (WS) at the height of 8m and 100 m; mass concentrations of (c) $PM_{2.5}$ and NR-$PM_1$ + BC and (d) submicron aerosol species. The extinction coefficient ($b_{ext}$) at 630 nm is shown in (c). Three events, i.e., Lunar New Year (LNY), Lunar Fifth Day (LFD) and Lantern Festival (LF) with significant influences of fireworks are marked in (c). In addition, the classified clean periods (CPs) and polluted events (PEs) are marked as shaded light blue and pink areas, respectively.

**Fig. 2.** Time series of $PM_1$ species (Org, $SO_4$, $NO_3$, $NH_4$, Chl, K, KCl, and BC) and meteorological variables (wind direction (100 m) and wind speed (8 m)) during three firework events, i.e., (a) Lunar New Year, (b) Lunar Fifth Day, and (c) Lantern Festival. The two blue arrow lines represent the starting and ending times of fireworks events.

**Fig. 3.** Correlation of $PM_1$ vs. $PM_{2.5}$ with the data segregated into three fireworks events (LNY, LFD, and LF) and non-fireworks periods (NFW). The blank circles represent FW data between 18:00 – 23:30 on 9 February which had large influences from NFW sources.

**Fig. 4.** Average chemical composition of $PM_1$ and OA from fireworks and background during three FW events.

**Fig. 5.** (a) Average mass spectra (MS) of OA during the firework period of Lunar New Year (23:30, 9 February – 3:30, 10 February) and the period of background (BG, 4:30 – 11:00, 10 February). (b) Comparison of the difference spectrum from (a), i.e., $MS_{FW+BG} - MS_{BG}$, with the average LV-OOA spectrum in Ng et al.(2011a). Note that five *m/z*'s, 37 ($^{37}Cl^+$), 58 ($NaCl^+$), 60 ($Na^{37}Cl^+$), 74 ($KCl^+$), and 76 ($K^{37}Cl^+$/ $^{41}KCl^+$) marked in the figure were dominantly from fragmentation of inorganic salts during fireworks.

**Fig. 6.** Box plots of (a) mass concentrations and (b) mass fractions of aerosol species for 9 pollution events marked in Fig. 1. The mean (cross), median (horizontal line), $25^{th}$ and $75^{th}$ percentiles (lower and upper box), and $10^{th}$ and $90^{th}$ percentiles (lower and upper whiskers) are shown for each box.

**Fig. 7.** Left panel: variations of chemical composition of (a) organics, SNA (=sulfate + nitrate + ammonium), and others (the rest species in $PM_1$); (b) SPM and PPM; and (c) SOA and POA as a function of $PM_1$ and organics loadings, respectively. The

middle and right panels show the diurnal profiles of composition and mass concentrations, respectively.

**Fig. 8.** (a) Average mass fraction of organics ($f_{Org}$) as a function of $PM_1$ mass, and (b) correlations of extinction coefficients ($PM_{2.5}$) vs. $PM_1$ for 9 pollution events (PEs) and 9 clean periods (CPs) marked in Fig. 1. The error bar represents one standard deviations of the average for each event.

**Fig. 9.** The average ratios of aerosol species, gaseous species, PM mass concentrations, extinction coefficient, and meteorological parameters between holiday (HD) and non-holiday (NHD) periods. Two different holidays, i.e., the official holiday of 9 – 15 February and the longer holiday of 7 – 20 February were used for averages. Also note that the averages were made by excluding clean periods and firework events during both HD and NHD days. The error bars are the standard errors of the ratios.

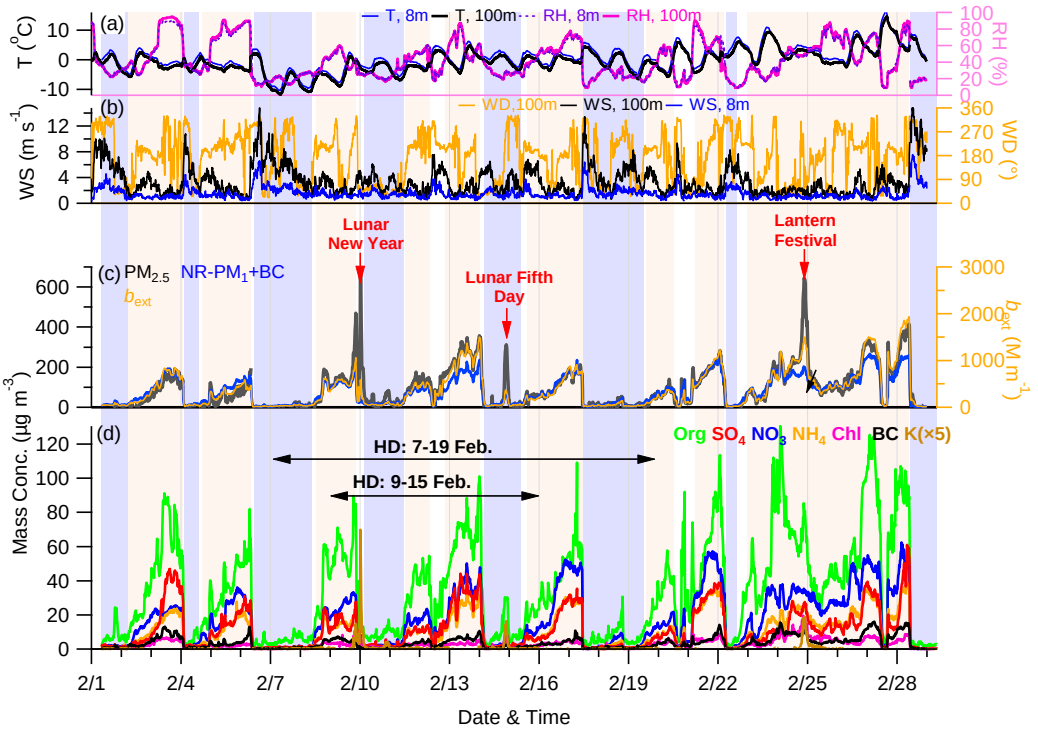


**Fig. 1.** Time series of meteorological parameters (a) relative humidity (RH) and temperature (T); (b) wind direction (WD) and wind speed (WS) at the height of 8m and 100 m; mass concentrations of (c) $PM_{2.5}$ and NR-$PM_1$ + BC and (d) submicron aerosol species. The extinction coefficient ($b_{ext}$) at 630 nm is shown in (c). Three events, i.e., Lunar New Year (LNY), Lunar Fifth Day (LFD) and Lantern Festival (LF) with significant influences of fireworks are marked in (c). In addition, the classified clean periods (CPs) and polluted events (PEs) are marked as shaded light blue and pink areas, respectively.

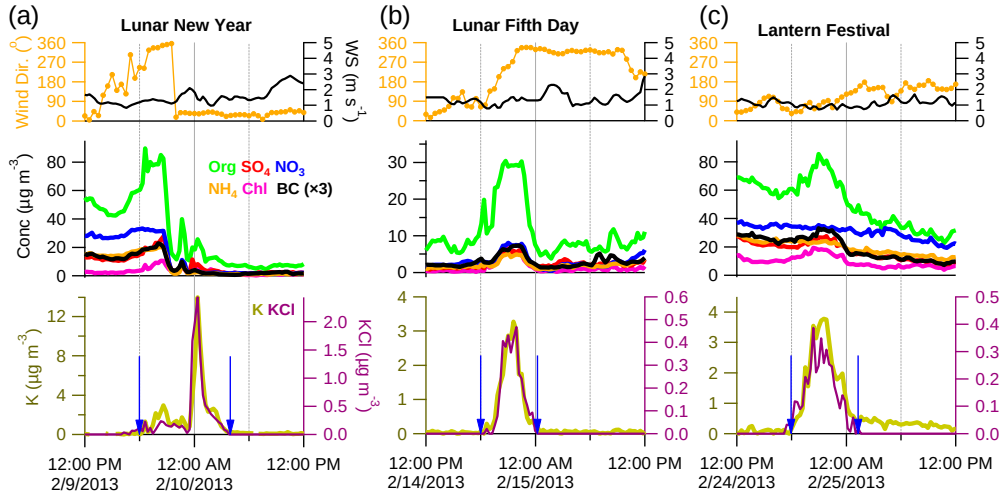

827 **Fig. 2.** Time series of $PM_1$ species (Org, $SO_4$, $NO_3$, $NH_4$, Chl, K, KCl, and BC) and
828 meteorological variables (wind direction (100 m) and wind speed (8 m)) during three
829 firework events, i.e., (a) Lunar New Year, (b) Lunar Fifth Day, and (c) Lantern
830 Festival. The two blue arrow lines represent the starting and ending times of fireworks
831 events.

832

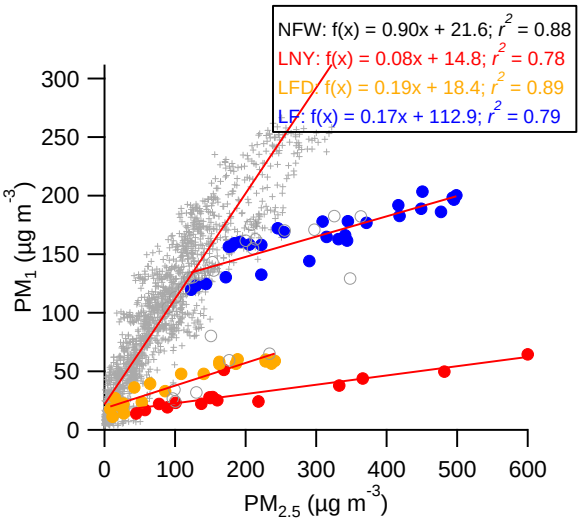


833

834 **Fig. 3.** Correlation of $PM_1$ vs. $PM_{2.5}$ with the data segregated into three fireworks
835 events (LNY, LFD, and LF) and non-fireworks periods (NFW). The blank circles
836 represent FW data between 18:00 – 23:30 on 9 February which had large influences
837 from NFW sources.

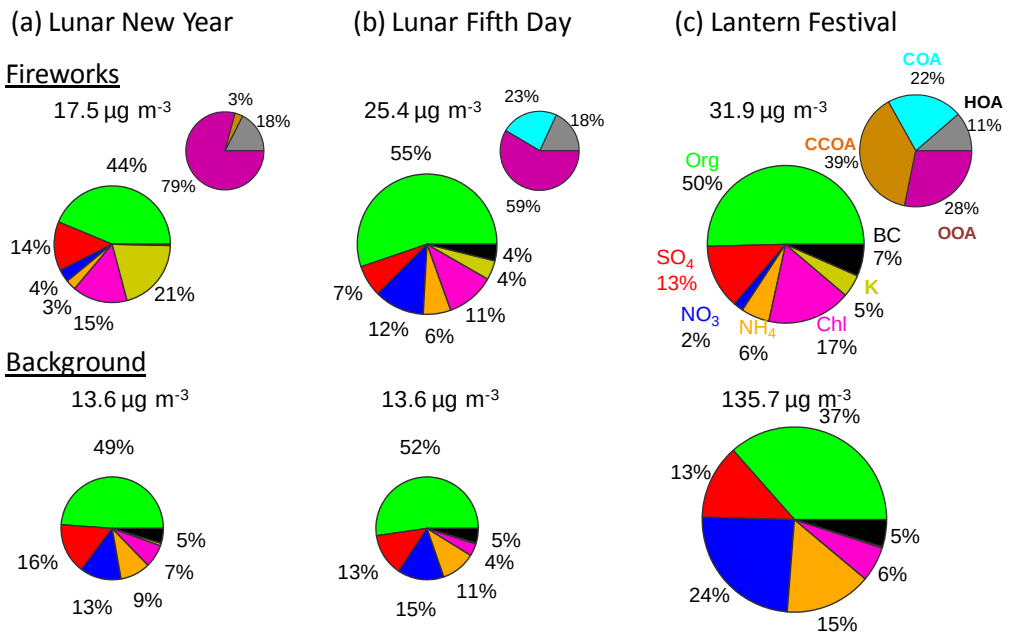


838

839 **Fig. 4.** Average chemical composition of $PM_1$ and OA from fireworks and
840 background during three FW events.

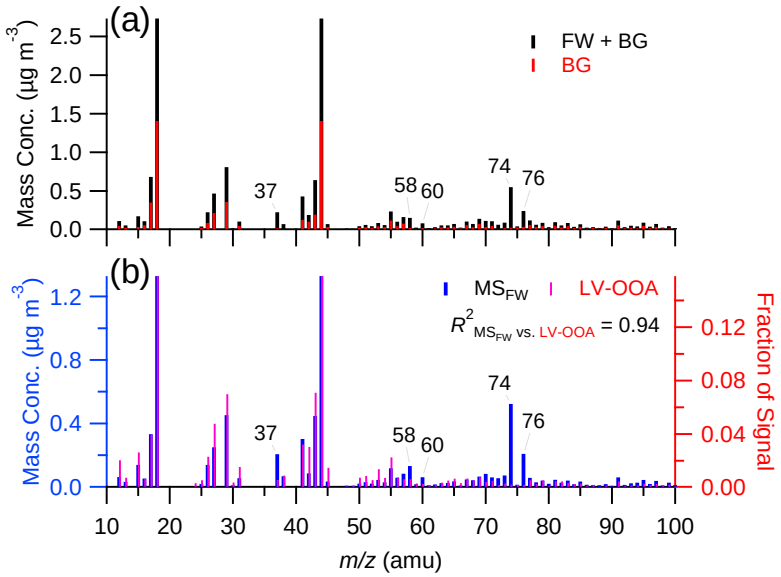


841

842 **Fig. 5.** (a) Average mass spectra (MS) of OA during the firework period of Lunar
843 New Year (23:30, 9 February – 3:30, 10 February) and the period of background (BG,
844 4:30 – 11:00, 10 February). (b) Comparison of the difference spectrum from (a), i.e.,
845 $MS_{FW+BG} - MS_{BG}$, with the average LV-OOA spectrum in Ng et al.(2011a). Note that
846 five *m/z*'s, 37 ($^{37}Cl^+$), 58 ($NaCl^+$), 60 ($Na^{37}Cl^+$), 74 ($KCl^+$), and 76 ($K^{37}Cl^+$/ $^{41}KCl^+$)
847 marked in the figure were dominantly from fragmentation of inorganic salts during
848 fireworks.

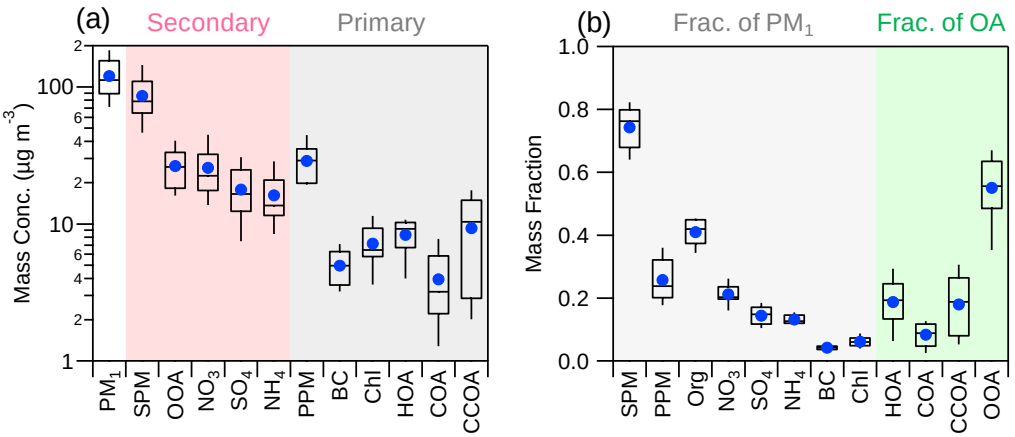


849

850 **Fig. 6.** Box plots of (a) mass concentrations and (b) mass fractions of aerosol species
851 for 9 pollution events marked in Fig. 1. The mean (cross), median (horizontal line),
852 25$^{th}$ and 75$^{th}$ percentiles (lower and upper box), and 10$^{th}$ and 90$^{th}$ percentiles (lower
853 and upper whiskers) are shown for each box.

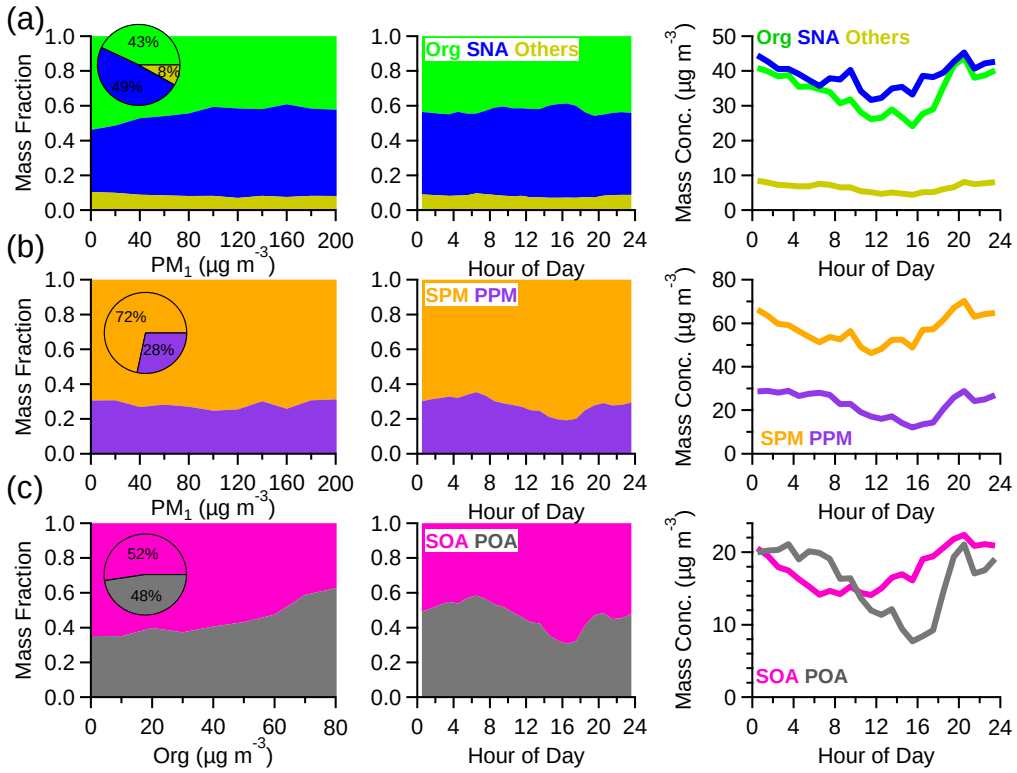


**Fig. 7.** Left panel: variations of chemical composition of (a) organics, SNA (=sulfate + nitrate + ammonium), and others (the rest species in $PM_1$); (b) SPM and PPM; and (c) SOA and POA as a function of $PM_1$ and organics loadings, respectively. The middle and right panels show the diurnal profiles of composition and mass concentrations, respectively.

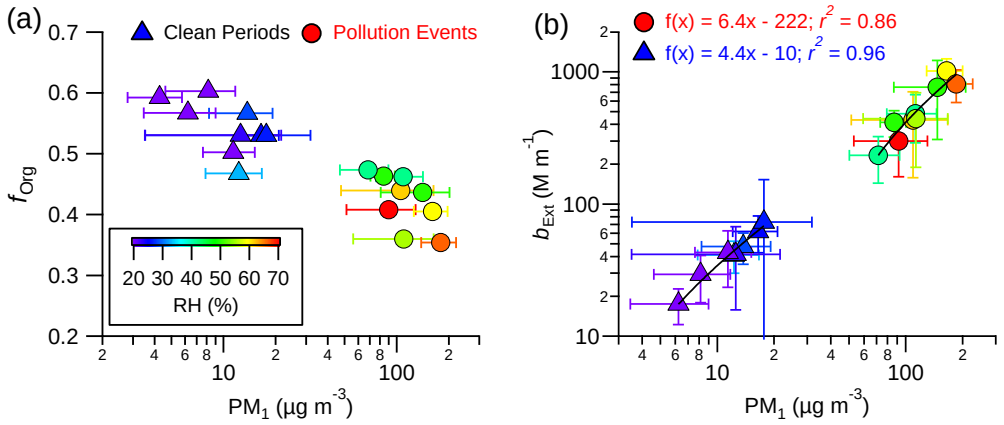


861

862 **Fig. 8.** (a) Average mass fraction of organics ($f_{Org}$) as a function of $PM_1$ mass, and (b)
863 correlations of extinction coefficients ($PM_{2.5}$) vs. $PM_1$ for 9 pollution events (PEs) and
864 9 clean periods (CPs) marked in Fig. 1. The error bar represents one standard
865 deviations of the average for each event.

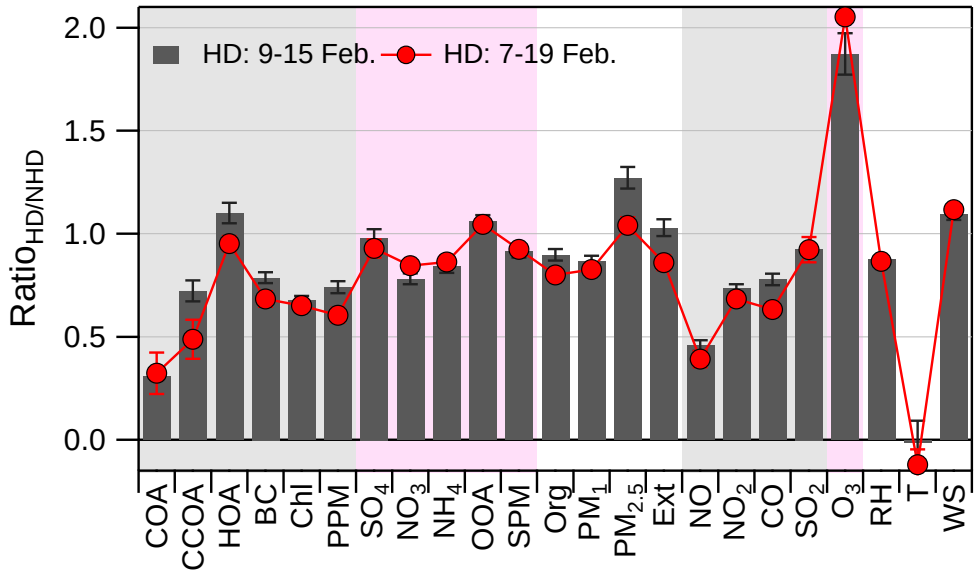


866

867 **Fig. 9.** The average ratios of aerosol species, gaseous species, PM mass
868 concentrations, extinction coefficient, and meteorological parameters between holiday
869 (HD) and non-holiday (NHD) periods. Two different holidays, i.e., the official
870 holiday of 9 – 15 February and the longer holiday of 7 – 20 February were used for
871 averages. Also note that the averages were made by excluding clean periods and
872 firework events during both HD and NHD days. The error bars are the standard errors
873 of the ratios.